Mapping the Unseen: Unified Promptable Panoptic Mapping with Dynamic Labeling using Foundation Models

Mohamad Al Mdfaa^{1 2} Raghad Salameh² Geesara Kulathunga³ Sergey Zagoruyko² Gonzalo Ferrer²

Abstract—In robotics and computer vision, semantic mapping remains a critical challenge for machines to comprehend complex environments. Traditional panoptic mapping approaches are constrained by fixed labels, limiting their ability to handle novel objects. We present Unified Promptable Panoptic Mapping (UPPM), which leverages foundation models for dynamic labeling without additional training. UPPM is evaluated across three comprehensive levels: Segmentation-to-Map, Map-to-Map, and Segmentation-to-Segmentation. Results demonstrate UPPM attains exceptional geometry reconstruction accuracy (0.61cm on the Flat dataset), the highest panoptic quality (0.414), and better performance compared to state-of-the-art segmentation methods. Furthermore, ablation studies validate the contributions of unified semantics, custom NMS, and blurry frame filtering, with the custom NMS improving the completion ratio by 8.27% on the Flat dataset. UPPM demonstrates effective scene reconstruction with rich semantic labeling across diverse datasets.

Index Terms—Semantic Scene Understanding, Panoptic Mapping, Open-Vocabulary Segmentation, Foundation Models, Deep Learning for Visual Perception

I. INTRODUCTION

ANOPTIC mapping is a key element in enabling robots to perceive and reconstruct their surroundings with better comprehension. However, existing methods [1], [2], [3] have issues due to their reliance on rigid predefined class sets, which limits their flexibility to unforeseen objects or dynamic environments. To be applicable in various real-world scenarios, these systems require either a large amount of labeled data [4], [5] or controlled environmental conditions. Integrating openvocabulary techniques [6], [7] is a potential way to improve robustness and generalizability.

Our key contributions include: (1) A Unified Promptable Panoptic Mapping (UPPM) framework¹ integrating foundation models into 3D panoptic mapping with semantically unified categories while preserving open-vocabulary labels; (2) Dynamic Labeling generating adaptive semantic descriptors for unseen environments, mapping open-vocabulary labels to structured categories with known sizes (sections III-B1 and III-B2); (3) Integration of semantic and geometric information demonstrating improved performance across three evaluation tiers: Segmentation-to-Map evaluation of segmentation quality impact on geometric reconstruction using PanMap [8] with different segmentation backbones across multiple datasets (section IV-A), Map-to-Map geometric reconstruction comparison with Kimera [9], PanMap [8], and DHP [10]

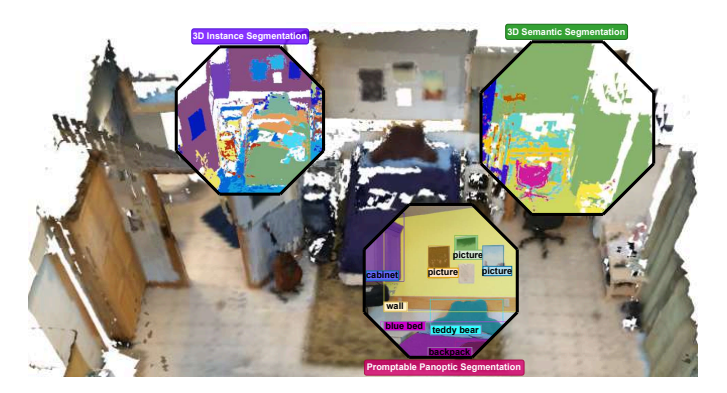


Fig. 1: UPPM dynamically generates object labels through open-vocabulary prompts, merging diverse labels into a unified semantic structure. Efficient post-processing, coupled with open-vocabulary object detection, ensures accurate segmentations and reconstructs a dynamically-labeled multi-resolution multi-TSDF map.

(section IV-B) attaining 16.44% accuracy improvement, and *Segmentation-to-Segmentation* panoptic segmentation quality assessment against state-of-the-art methods (section IV-C) attaining highest panoptic quality (0.414); and (4) Comprehensive ablation studies validating unified semantics (section V-A), custom NMS (section V-B), and blurry frame filtering (section V-C).

II. RELATED WORK

Semantic mapping has evolved from dense approaches [11], [12] to object-centric methods [3], [2] and panoptic mapping [8], [1]. While these methods provide comprehensive scene understanding, they rely on fixed semantic classes, limiting adaptability to novel objects. Recent open-vocabulary segmentation methods [4], [13], [14] enable dynamic semantic understanding but lack integration with 3D mapping frameworks.

Foundation models have revolutionized computer vision tasks through vision-language models [15], [16] and segmentation models [17]. Recent open-vocabulary segmentation methods [13], [14] have demonstrated remarkable capabilities in recognizing novel objects without predefined categories. However, these methods focus solely on 2D segmentation and lack integration with 3D mapping frameworks, limiting their applicability in robotic perception tasks.

As shown in table I, current methods are limited by either fixed-set vocabularies or incomplete scene representations. While fixed-set methods like PanMap [8] and Kimera [9] provide panoptic representations, they cannot handle novel objects. Open-vocabulary approaches like ConceptFusion [7] enable flexible semantics but lack unified semantic structures for consistent object understanding. UPPM bridges this gap by leveraging foundation model advances to enable dynamic

¹⁻ Correspondence: mohamad.almdfaa@skoltech.ru

²⁻ Center for AI Technology, Skolkovo Institute of Science and Technology, Skolkovo, Moscow, Russia

³⁻ School of Computer Science, University of Lincoln, United Kingdom

¹Project webpage: https://unified-promptable-panoptic-mapping.github.io



Fig. 2: UPPM enables interactive scene exploration and object retrieval, employing query post-processing and semantic textual similarity for enhanced accuracy. By displaying an environment with a table and dynamic labels attached to it, the application demonstrates the UPPM reconstructed map. Dynamic labels enable the system to respond to four distinct user prompts by pointing to the same object.

label generation within a unified panoptic mapping framework, providing both geometric accuracy and semantic flexibility for interactive robotic perception.

III. METHODOLOGY

UPPM addresses the visual semantic mapping problem by utilizing foundation models for dynamic label generation. The mapping pipeline follows a systematic multi-stage process: First, rich semantic descriptions are extracted from visual inputs using vision-language models. Second, these descriptions are mapped to structured semantic categories while preserving their descriptive richness. Third, precise open-vocabulary object detection and segmentation is performed using these semantic descriptors. Fourth, all components are integrated into a unified panoptic map that maintains both geometric accuracy and semantic consistency. The complete mapping pipeline is shown in fig. 3.

A. Problem Formulation

Given a sequence of posed RGBD images $\mathcal{I} = \{I_1, \dots, I_T\}$ where each $I_t = (R_t, D_t, P_t)$ consists of an RGB image $R_t \in \mathbb{R}^{H \times W \times 3}$, a depth image $D_t \in \mathbb{R}^{H \times W}$, and a camera pose $P_t \in SE(3)$, our goal is to construct a unified promptable panoptic map \mathcal{M} that satisfies the following objectives:

- 1) **Geometric Reconstruction:** Generate an accurate 3D reconstruction of the environment represented as a multiresolution multi-TSDF map \mathcal{M}_g .
- 2) **Dynamic Labeling with Unified Semantics:** Construct the set of dynamic labels \mathcal{M}_d by leveraging vision-language models to generate rich semantic descriptions and mapping them to structured semantic descriptors.

Specifically, assign a dynamic label $d_i \in \mathcal{M}_d$ to each detected object $o_i \in \mathcal{O}$, where \mathcal{O} is the set of all objects in the scene. Such dynamic label $d_i = \langle o_i, E(o_i), \hat{c}_i, \hat{s}_i \rangle$ is a tuple containing: the original open-vocabulary label o_i , the corresponding dense vector embedding $E(o_i)$, the assigned unified category $\hat{c}_i \in \mathcal{C}$, and the predicted size \hat{s}_i , where \mathcal{C} is the set of fixed

unified categories (i.e., COCO-Stuff classes [21]). COCO-Stuff classes were chosen as the fixed unified categories due to their comprehensive coverage of common indoor objects and well-established hierarchy, providing a robust foundation for semantic mapping tasks. The final output is a unified promptable panoptic map $\mathcal{M} = (\mathcal{M}_g \bigoplus \mathcal{M}_d)$, where the fusion operator \bigoplus combines geometric reconstruction \mathcal{M}_g with dynamic labels \mathcal{M}_d into a unified volumetric representation integrating spatial and semantic information. The mapping process operates at interactive rates while maintaining accuracy in both geometric reconstruction and unified semantic labeling.

B. Dynamic Label Generation and Segmentation

As shown in fig. 3, the per-frame processing pipeline consists of three sequential modules that generate structured dynamic labels from RGB images as input. The first module, Visual-Linguistic Feature Extraction++ (VLFE++), uses vision-language models to generate open-vocabulary labels from images. The second module, Semantic-Textual Similarity (STS), maps these labels to unified categories. The third module, Open-vocabulary Object Detection and Segmentation, uses these enhanced labels to produce object bounding boxes and instance masks for panoptic map construction.

1) Visual-Linguistic Feature Extraction++ (VLFE++): VLFE++ leverages vision-language models to generate comprehensive open-vocabulary labels from visual information.

As shown in fig. 3, VLFE++ employs a multi-stage process to generate rich semantic descriptions:

- Visual Linguistic Features Extraction (VLFE): We employ Tag2Text [15], a vision-language pre-training framework, which provides strong semantic guidance. Tag2Text generates comprehensive captions and diverse tag categories with enhanced zero-shot performance, producing rich semantic descriptions for subsequent processing steps.
- Part-Of-Speech (POS) Tagging: We process the captions using an average perceptron network [22] to extract nouns, noun phrases, and associated adjectives, providing rich contextual information about detected objects. This list of object names and their descriptive attributes is then used as input for the next step, lemmatization.
- Lemmatization: We normalize extracted words through lemmatization [23], converting derived forms to their base form (e.g., 'apples' → 'apple'), producing canonical object labels for subsequent processing.

The generated open-vocabulary labels serve as input for the next pipeline component, STS.

2) Semantic-Textual Similarity (STS): STS maps open-vocabulary labels to structured unified categories while preserving descriptive richness. Let \mathcal{O}_{vocab} be the set of open-vocabulary labels from VLFE++ and \mathcal{C} be the set of fixed unified categories, where each class $(c_i \in \mathcal{C})$ has a corresponding size attribute (s_i) , which takes one of three values small (s=1), medium (s=2), or large (s=3). Our goal is to determine the most appropriate unified category \hat{c} for any given open-vocabulary label $o \in \mathcal{O}_{vocab}$:

TABLE I: UPPM is a unified framework to combine panoptic 3D representations with the flexibility of open-vocabulary semantics. Unlike prior work, which is limited to either fixed-set vocabularies or incomplete scene representations (e.g., non-panoptic or lacking semantic unification), UPPM delivers on all critical capabilities for a truly generalizable mapping system.

	Method	Panoptic Representation	Open-Vocabulary	Semantic Unification	Key Contribution
Fixed-Set	SemanticFusion [11]	✓	Х	Pre-defined	Dense Semantic Fusion
Semantic Mapping	SLAM++ [3]	×	X	Pre-defined	Object-Level SLAM
Semantic Mapping	Panoptic Fusion [1]	✓	X	Pre-defined	Volumetric Semantic Mapping at the Level of Stuff and Things
	Kimera [9]	✓	X	Pre-defined	3D Dynamic Scene Graphs Generation
	PanMap [8]	✓	×	Pre-defined	Submap-based spatio-temporally consistent volumetric mapping
	ConceptFusion [7]	1	1	Х	Multimodal 3D Mapping
Open-Vocabulary	ConceptGraphs [18]	×	✓	×	3D Scene Graph Generation
Semantic Mapping	OVIR-3D [19]	×	✓	X	3D Instance Retrieval
0	OpenMask3D [20]	X	✓	×	Zero-Shot 3D Instance Segmentation
	UPPM (Ours)	1	1	1	Unified Promptable Panoptic Mapping

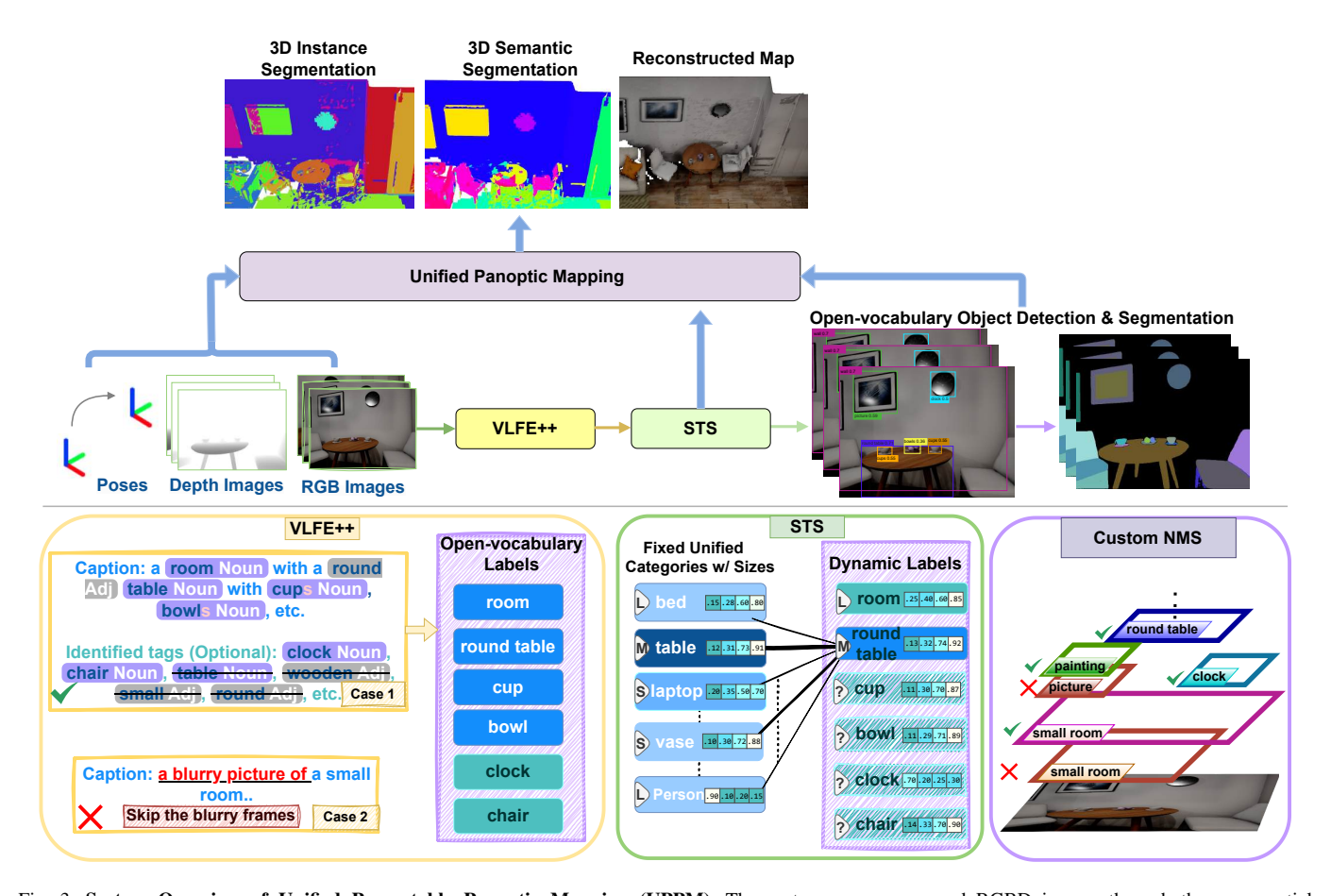


Fig. 3: System Overview of Unified Promptable Panoptic Mapping (UPPM). The system processes posed RGBD images through three sequential components. VLFE++ generates open-vocabulary labels from RGB inputs. STS maps these labels to unified categories and predicts object sizes, producing dynamic labels $d_i = \langle o_i, E(o_i), \hat{c}_i, \hat{s}_i \rangle$. Open-vocabulary Object Detection & Segmentation uses these dynamic labels with custom NMS to predict object bounding boxes and instance masks. The final output integrates geometric reconstruction \mathcal{M}_g with dynamic labels \mathcal{M}_d to produce a unified promptable panoptic map $\mathcal{M} = (\mathcal{M}_g \bigoplus \mathcal{M}_d)$.

$$\hat{c} = \operatorname*{arg\,max}_{c \in \mathcal{C}} \cos(E(o), E(c)), \tag{1}$$

where $\cos(\cdot)$ denotes the cosine similarity between embeddings and $E(\cdot)$ denotes the embedding function that maps labels to vector representations. The predicted size $\hat{s}=s_{\hat{c}}$ is inherited from the assigned unified category \hat{c} . To generate these embeddings, we employ MPNet [24], which provides robust semantic representations. After obtaining the embeddings, we conduct a semantic search [25] using cosine similarity to select the closest match among the unified categories. For

each open-vocabulary label $o_i \in \mathcal{O}_{\text{vocab}}$, STS generates the corresponding dynamic label $d_i \in \mathcal{M}_d$ by combining the original label with its semantic assignments:

$$d_i = \langle o_i, E(o_i), \hat{c}_i, \hat{s}_i \rangle, \tag{2}$$

where o_i is the original open-vocabulary label from VLFE++, $E(o_i)$ is its embedding vector representation, \hat{c}_i is the assigned unified category (computed using (1)), and \hat{s}_i is the predicted size. Through this structure, each dynamic label stores both human-readable and machine-readable semantic information, enabling advanced downstream processing while

maintaining descriptive richness. Such dynamic labels are used as input for the open-vocabulary object detector.

- 3) Open-vocabulary Object Detection and Segmentation: UPPM employs Grounding-DINO [16] as the object detector, leveraging its capability to process curated dynamic labels for open-vocabulary object detection. Grounding-DINO generates precise bounding boxes that serve as input prompts for the Segment Anything Model (SAM) [17], enabling the creation of high-quality instance masks for each detected object in the scene. Furthermore, as shown in table VI, a custom Non-Maximum Suppression (NMS) technique is proposed to address the open-vocabulary detection challenges [16]. While traditional NMS approaches like per-class NMS [26] remove redundant bounding boxes based on Intersection-over-Union (IoU) and confidence scores within the same class, our custom NMS handles two additional scenarios:
 - Prioritizing caption-derived labels: When overlapping bounding boxes have different labels but belong to the same unified category, we prioritize the box whose label originates from the image caption over those derived from the identified tags, as shown in fig. 3. This contextaware selection leverages the richer semantic information provided by captions compared to identified tags.
 - 2) **Standard duplicate removal:** For overlapping bounding boxes b_a, b_b with identical labels where $IoU(b_a, b_b) \ge \tau$, we apply conventional suppression based on confidence scores, retaining the box with higher detection confidence.

C. Unified Panoptic Mapping

Building upon the object detection and segmentation results, we integrate these outputs into a comprehensive 3D representation. Traditional panoptic mapping approaches rely on fixed semantic categories, limiting their ability to handle novel objects. Our Unified Panoptic Mapping extends beyond these limitations by integrating dynamic labels while maintaining semantic consistency through unified categorization. We build upon the object-centric mapping framework introduced in [8], specifically leveraging its submap-based architecture. Submaps are localized volumetric representations that divide large-scale environments into smaller, manageable parts, where each submap contains geometric and semantic data including panoptic information, object instances, and semantic categories, along with transformation and tracking data. This structure enables efficient processing of large-scale environments while significantly reducing computational complexity. Our key contribution is the enrichment of each submap with dynamic labels, as shown in fig. 4. While traditional submaps store fixed semantic labels, our approach enables each submap to contain its associated dynamic labels, allowing for flexible object understanding without sacrificing semantic consistency. The Unified Panoptic Mapping component takes as input posed RGBD data, dynamic labels, detected objects, and panoptic segmentation, reconstructing the Unified Promptable Panoptic Map (UPPM) \mathcal{M} by integrating this information into the enhanced submap structure. The resulting map is accurately reconstructed and enriched with dynamic labels, facilitating downstream tasks such as navigation and localization.

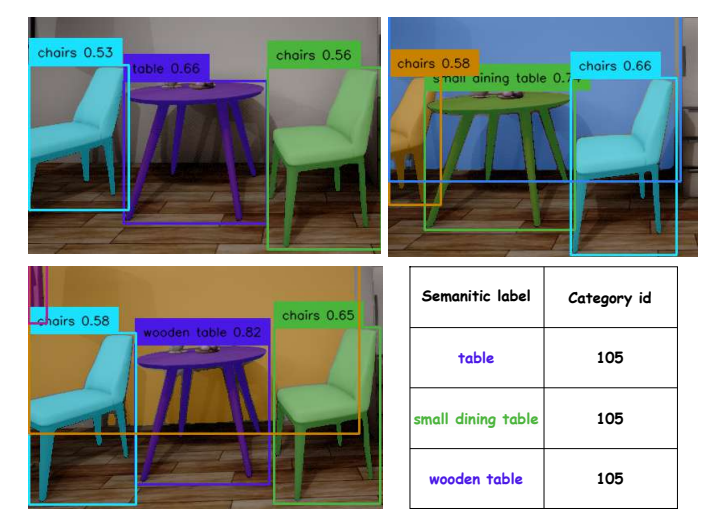


Fig. 4: Unified Semantics in Action: Three sequential frames featuring the same table with distinct dynamic labels – "table", "small dining table", and "wooden table". Despite varied descriptions, the unified semantics maintains a consistent class ID across all instances, matching that of the unified category "table". This approach ensures semantic cohesion while allowing for more specific dynamic descriptors.

IV. EXPERIMENTS

The experimental evaluation of UPPM is organized into three tiers to assess different aspects of system performance:

- (1) Segmentation-to-Map Evaluation: UPPM is validated against PanMap [8] deployed with different segmentation backbones including MaskDINO [4], OpenSeeD [13], OMG-Seg [14], and the human-annotated Ground Truth Segmentation (GTS) provided with each dataset [27], [28], [8] across three datasets: ScanNet v2, RIO, and Flat. Performance is evaluated using geometric reconstruction metrics (Accuracy, Completeness, Hausdorff distance, Completion Ratio, Chamfer distance), fine-detail assessment metrics (F1-Score), and frame rate (FPS). The selected datasets provide complementary evaluation scenarios: Flat [8] is a simulated dataset emphasizing reconstruction accuracy, RIO [28] is a real-world noisy dataset testing robustness to noise and error propagation, and ScanNet v2 [27] serves as a stringent real-world benchmark with diverse semantic categories. MaskDINO represents a closedset model with 1203 categories [29], while OpenSeeD and OMG-Seg are open-vocabulary methods enabling comparison with our dynamic labeling approach.
- (2) Map-to-Map Evaluation: The Flat dataset is used to compare UPPM against state-of-the-art mapping pipelines including Kimera [9], PanMap [8], and DHP [10]. Performance is assessed using geometric reconstruction metrics: Accuracy, Completeness and Chamfer-L1 distance, which represents the Chamfer distance computed using L1 norm for robust overall reconstruction quality assessment.
- (3) Segmentation-to-Segmentation Evaluation: The Flat dataset is employed to assess UPPM panoptic segmentation quality against state-of-the-art segmentation baselines including MaskDINO [4], OpenSeeD [13], OMG-Seg [14], and

Detectron2 [30], using the panoptic segmentation metrics (Panoptic Quality, Recognition Quality, Segmentation Quality, mean Average Precision).

All experiments were conducted on a server featuring an NVIDIA A100 80GB GPU and 256GB of RAM, ensuring consistent evaluation conditions across all methods and maintaining reproducibility of results.

A. Segmentation-to-Map Evaluation

The impact of segmentation quality on geometric reconstruction is assessed by comparing UPPM with PanMap [8], each deployed with different segmentation backbones: MaskDINO [4], OpenSeeD [13], OMG-Seg [14], and GTS.

UPPM achieves strong performance across multiple metrics (table II). The proposed method attains optimal accuracy on RIO (1.55 cm) and Flat (0.61 cm) with competitive performance on ScanNet v2 (3.30 cm), where Accuracy measures how close reconstructed points are to ground truth, calculated as mean absolute error from reconstruction (R) to ground truth (G). This improved accuracy on RIO shows UPPM's robustness to motion blur and sensor noise common in realworld datasets. To assess how thoroughly the reconstruction captures the ground truth scene, Completeness is defined as the mean absolute error from ground truth (G) to reconstruction (R). UPPM attains outstanding completeness on Flat (1.10 cm)and competitive performance on ScanNet v2 (1.78 cm) and RIO (1.19 cm). This pattern reflects the influence of dataset characteristics: Flat [8], being simulated, enables precise reconstruction and higher completeness, while the real-world conditions and noise in RIO [28] and ScanNet v2 [27] make achieving high completeness more challenging. The metrics Accuracy and Completeness are asymmetrical, as distances from ground truth points (G) to reconstructed map points (R)may differ from R to G. These metrics compute distances by comparing each point in one set to its nearest neighbor in the other. A larger Accuracy component suggests potential inaccuracies in reconstruction, while a larger Completeness component suggests potential incompleteness.

To estimate how completely the reconstruction covers the ground truth, we use the *Completion Ratio*, defined as the percentage of observed ground truth points reconstructed within a $5\,cm$ threshold. UPPM achieves strong completion ratios (81.42% on ScanNet v2, 74.14% on RIO, 70.76% on Flat). The higher completion ratio on ScanNet v2 reflects the ability to leverage higher quality data and more diverse semantic categories, while the lower ratio on RIO indicates the challenge of noisy real-world data.

To quantify geometric similarity between the reconstructed and ground truth point clouds, *Chamfer distance* $d_{\rm ch}(G,R)$ is used. This metric provides an overall assessment of how closely the reconstructed and ground truth point clouds match:

$$d_{\text{ch}}(G, R) = \underbrace{\sum_{g \in G} \min_{r \in R} \|g - r\|_2^2}_{\text{Completeness}} + \underbrace{\sum_{r \in R} \min_{g \in G} \|g - r\|_2^2}_{\text{Accuracy}}$$
(3)

UPPM achieves exceptional Chamfer distance on RIO and competitive performance on ScanNet v2 and Flat (ScanNet v2:

12.64 cm, RIO: 5.65 cm, Flat: 2.64 cm). This lower Chamfer distance reflects the effectiveness of the multi-resolution Multi-TSDF approach, which balances accuracy and completeness. The substantial improvements on RIO indicate UPPM's robustness to motion blur and sensor noise, while competitive performance on ScanNet v2 shows its ability to handle complex real-world scenes with diverse semantic categories.

To estimate the worst-case reconstruction error, we use the *Hausdorff distance* (d_H) , as defined in eq. (4). This metric measures the greatest distance from a point in one set to the closest point in the other set:

$$d_H(G, R) = \max\left(\max_{g \in G} \min_{r \in R} \|g - r\|_2, \max_{r \in R} \min_{g \in G} \|r - g\|_2\right)$$
(4)

UPPM achieves competitive Hausdorff distance performance with optimal performance on RIO (10.05 cm vs 18.55-21.60 cm from competitors), demonstrating UPPM's robustness in minimizing worst-case reconstruction errors. The Hausdorff distance on Flat (4.75 cm) highlights how the controlled environment helps minimize outlier errors. The strong performance on ScanNet v2 (25.53 cm) demonstrates UPPM's ability to manage complex scenes with varied geometric structures while keeping worst-case errors within reasonable limits.

To measure the ability to reconstruct fine-grained details while accounting for both false positives and false negatives, F1-Score is calculated after removing background classes (e.g., floor, ceiling, wall). UPPM achieves 2.27 FPS on Flat (batch size 1), demonstrating computational efficiency suitable for real-time applications. UPPM attains the highest F1-score (79.54%), indicating better fine-detail reconstruction. This result is enabled by the custom NMS strategy, which removes duplicates while preserving details, and by dynamic labeling that improves coverage without over-segmentation.

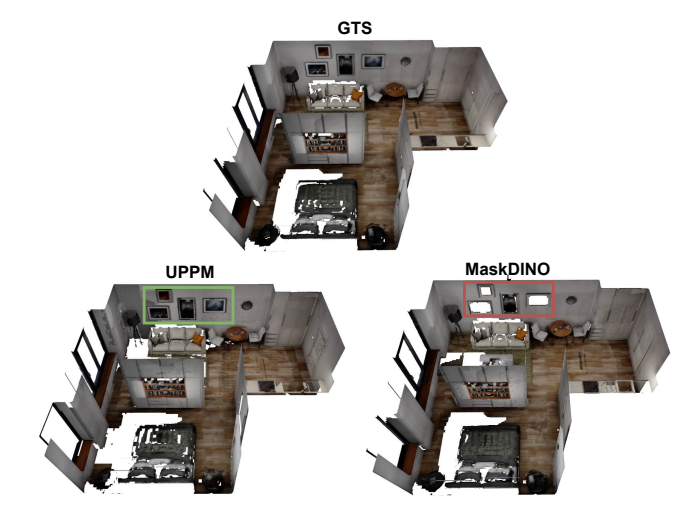


Fig. 5: Qualitative comparison of map reconstruction on the Flat dataset [8]. While MaskDINO achieves a high completion ratio, it fails to reconstruct fine-grained details like wall paintings. UPPM, in contrast, captures these elements, demonstrating enhanced detailed scene understanding.

The qualitative analysis reveals important insights about reconstruction quality. As shown in fig. 5, while MaskDINO

achieves better completion ratio on some datasets, it demonstrates better reconstruction for large structures like walls and floors but fails to capture intricate details such as paintings on walls, which hold significant semantic value. Conversely, UPPM successfully reconstructs these fine-grained elements, demonstrating its high capability in detailed scene understanding.



Fig. 6: Comparative visualization on the RIO dataset. **Top:** Ground truth segmentation with corresponding colored map. **Bottom:** UPPM's output, showing refined segmentation and enhanced detail in both spatial and colored representations, highlighting its better performance in complex scenes.

Overall Performance Analysis For comprehensive analysis across diverse scenarios, we present aggregated evaluation results for all datasets using a weighted average approach. As shown in fig. 7, UPPM shows robust performance across multiple metrics including Completion Ratio, F1-score, Chamfer distance, Hausdorff distance, and Accuracy. The Chamfer distance metric is more reliable and less sensitive to outliers than individual Accuracy and Hausdorff distance components, clearly demonstrating that UPPM outperforms other closed-set [4] and open-vocabulary [13], [14] approaches in overall performance.



Fig. 7: Overall performance of UPPM. Left y-axis: Completion Ratio and F1-Score (higher is better). Right y-axis: Chamfer distance, Hausdorff distance, and Accuracy (lower is better).

B. Map-to-Map Evaluation

UPPM is compared against leading mapping pipelines including Kimera [9], PanMap [8], and DHP [10], representing state-of-the-art approaches in volumetric and semantic mapping. The Chamfer-L1 metric provides robust assessment of overall reconstruction quality by measuring geometric fidelity with reduced sensitivity to outliers compared to L2 norm.

UPPM achieves remarkable performance across all geometric metrics (table III), with exceptional accuracy $(0.61\,cm)$, completeness $(1.10\,cm)$, and Chamfer-L1 distance $(1.71\,cm)$. The enhanced accuracy is enabled by the submap-based architecture that supports localized optimization, combined with semantic–geometric integration that improves object-level reconstructions. The better completeness $(1.10\,cm)$ vs $6.48-7.63\,cm$ from competitors) demonstrates UPPM's ability to capture more complete scene geometry through its multi-resolution Multi-TSDF approach, while the outstanding Chamfer-L1 distance $(1.71\,cm)$ vs $3.62-4.24\,cm$ reflects the balanced optimization between accuracy and completeness. These results demonstrate UPPM's effectiveness in producing geometrically accurate maps while maintaining the benefits of dynamic semantic labeling.

C. Segmentation-to-Segmentation Evaluation

As shown in table IV, UPPM achieves the highest *Panoptic* Quality (PQ) (0.414), Recognition Quality (RQ) (0.475), and mean Average Precision (mAP) across multiple IoU thresholds, with competitive Segmentation Quality (SQ) (0.845). The better PQ and RQ performance stems from the unified semantics approach that reduces label ambiguity and improves instance recognition, while the competitive SO reflects the precision of instance masks guided by dynamic labels and enhanced duplicate suppression through custom NMS. The highest mAP scores across all IoU thresholds (0.549, 0.521, 0.475) demonstrate UPPM's consistent performance in object detection and localization, outperforming MaskDINO (0.546, 0.516, 0.470) and other competitors. These results validate the effectiveness of the dynamic labeling approach in producing high-quality panoptic segmentations that maintain both semantic consistency and spatial accuracy.

V. ABLATION STUDIES

The objective of the ablation studies is to gain a deeper understanding of the contributions made by different components in UPPM.

A. Unified Semantics

In this study, we examine the effects of deactivating the unified semantic mechanism, which we call PPM (Promptable Panoptic Mapping), to assess the impact of unified semantics on map reconstruction. As shown in table V, UPPM outperforms PPM across all metrics on the Flat dataset, achieving better completion, accuracy, and Chamfer distance, in addition to the added benefit of unified semantics. As shown in fig. 8, PPM lacks dynamically labeled classes, leading to ambiguity when many semantic categories attach to the same object. In comparison, UPPM exhibits consistent behavior by reliably assigning semantic classes to objects while maintaining richness in dynamic labeling.

B. Non-Maximum Suppression

We compare traditional NMS with our custom NMS on Flat (tables VI and VII).

TABLE II: Quantitative evaluation across all datasets. All baselines use the PanMap framework [8] with different segmentation backbones. Abbreviations: Comp. = Completion, Acc. = Accuracy, Chamf. = Chamfer distance, Haus. = Hausdorff distance, C.R. = Completion Ratio, F1 = F1-Score, FPS = Frames Per Second. The highlight colors indicate the ranking for each metric: best, second best, and third best.

	ScanNet v2			RIO			Flat										
Method	Comp. [cm](↓)	Acc. [cm](↓)	Chamf. [cm](↓)	Haus. [cm](↓)	C.R. [%](†)	Comp. [cm](↓)	Acc. [cm](↓)	Chamf. [cm](↓)	Haus. [cm](↓)	C.R. [%](↑)	Comp. [cm](↓)	Acc. [cm](↓)	Chamf. [cm](↓)	Haus. [cm](↓)	C.R. [%](↑)	F1 (↑)	FPS (†)
GTS	1.38	2.80	9.46	18.53	82.5	1.23	1.91	10.25	21.43	77.09	1.27	0.66	3.05	5.60	71.30	-	-
MaskDINO	1.81	4.40	16.76	35.65	81.21	1.28	1.97	9.16	18.55	76.63	1.26	0.68	3.08	5.58	71.69	76.01	5.95
OpenSeeD	1.64	3.64	13.8	28.95	80.95	1.15	1.89	8.91	18.50	74.39	1.18	0.653	2.71	4.78	66.5	76.43	1.43
OMG-Seg	1.54	4.67	16.46	36.00	76.01	0.92	2.95	9.86	21.60	34.54	1.14	0.67	2.62	4.53	68.03	77.99	1.33
UPPM (Ours)	1.78	3.30	12.64	25.53	81.42	1.19	1.55	5.65	10.05	74.14	1.1	0.61	2.64	4.75	70.76	79.54	2.27

TABLE III: Geometric reconstruction quality on the Flat dataset. UPPM is compared against state-of-the-art methods, demonstrating exceptional performance in accuracy, completeness, and Chamfer-L1 distance.

Method	Acc. [cm]↓	Comp. [cm]↓	Chamfer-L1 [cm]↓
Kimera	0.76	6.48	3.62
Panmap	0.86	7.63	4.24
DHP	0.73	6.58	3.65
UPPM (Ours)	0.61	1.1	1.71

TABLE IV: Panoptic segmentation quality on the Flat dataset. UPPM is evaluated against other methods on key metrics, with highlight colors indicating performance ranking: best, second best, and third best.

Method	PQ ↑	RQ ↑	$\mathbf{SQ}\uparrow$	mAP-(0.3) ↑	mAP-(0.4) ↑	mAP-(0.5) ↑
MaskDINO	0.406	0.470	0.851	0.546	0.516	0.470
OMG-Seg	0.164	0.200	0.498	0.287	0.244	0.200
Detectron2	0.343	0.432	0.787	0.499	0.473	0.432
UPPM (Ours)	0.414	0.475	0.845	0.549	0.521	0.475

TABLE V: Results of Quantitative Ablation Experiments on Flat Dataset. Abbreviations: Comp. = Completion, Acc. = Accuracy, Chamf. = Chamfer distance

Method	Comp.	Acc.	Chamf.
	[cm](↓)	[cm](↓)	[cm](↓)
UPPM UPPM with tags	1.1 1.2	0.61 0.63	2.64 2.77
PPM PPM with tags	1.18	0.65	2.79
	1.22	0.66	2.92

Custom NMS improves the completion ratio by 8.27% (62.11% \rightarrow 70.38%) at unchanged Chamfer (2.79 cm), widening reconstructed coverage by removing overlaps and redundancies. The 8.27% gain arises from context-aware suppression that prioritizes caption-derived labels and removes duplicates across semantically equivalent detections. This improvement demonstrates that our custom NMS strategy effectively balances duplicate removal with coverage preservation, achieving better completion without sacrificing geometric accuracy.

C. Blurry Frames Filtering

We skip frames flagged as blurry by the caption model (fig. 3). This filtering strategy has negligible effect on Flat, small impact on ScanNet v2 (0.84% flagged), and a larger effect on RIO (3% flagged; manual inspection suggests > 21% affected). On RIO, UPPM reduces Chamfer distance by 16.675% and increases completion ratio by 6.47%. These gains arise because filtering out low-quality frames reduces geometric inconsistencies and error accumulation during fusion.

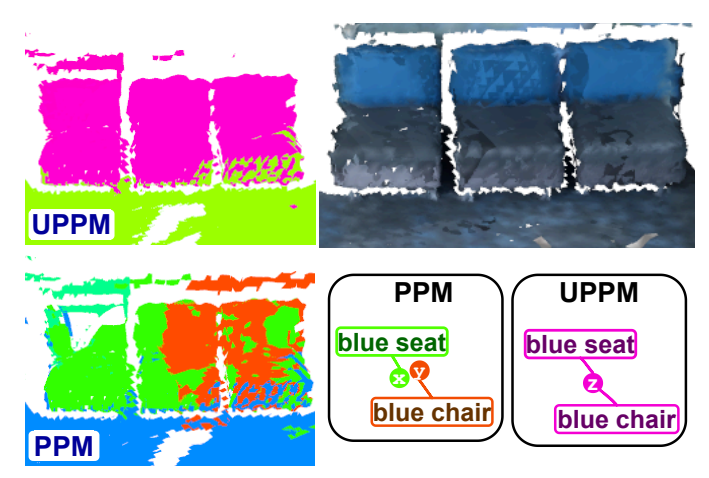


Fig. 8: Qualitative comparison of PPM vs. UPPM on 3D semantic segmentation. PPM struggles with semantic ambiguity, while UPPM consistently assigns class labels while preserving rich dynamic descriptions. The predicted semantic classes are represented by x,y,&z.

TABLE VI: Comparison of traditional NMS [26] and our custom NMS on the Flat dataset. Custom NMS demonstrates better performance across all metrics.

Method	Precision [%](\uparrow)	Recall [%](\uparrow)	F1-Score [%](†)
NMS [26]	91.3	63.64	75.0
Custom NMS (Ours)	94.6	100.0	97.22

TABLE VII: Quantitative NMS results on the Flat dataset. The custom NMS significantly improves the completion ratio while maintaining the same Chamfer distance.

Method	Chamfer dist. [cm](\downarrow)	Comp. Ratio [<5cm %](†)
PPM	2.79	70.38
PPM w/o NMS	2.79	62.11
Enhancement	0.00	+8.27 %

D. Identified Tags

As shown in fig. 3, we offer the option to use the identified tags in the pipeline. For the Flat dataset, as shown in table V, integrating the identified tags to both PPM and UPPM results in marginal improvement in completion ratio and all other metrics in the case of UPPM. This demonstrates that semantic information adds to more comprehensive scene knowledge.

VI. CONCLUSION

We introduced Unified Promptable Panoptic Mapping (UPPM), a framework that unifies open-vocabulary perception with panoptic 3D mapping by leveraging foundation models

to produce dynamic labels and enforcing a consistent semantic structure. The system integrates vision-language guided label generation, semantic unification, and open-vocabulary detection and segmentation into a submap-based multi-resolution multi-TSDF representation, yielding maps that couple geometric fidelity with flexible, human-interpretable semantics. Extensive evaluation and ablation studies indicate that the approach is effective across diverse datasets and segmentation backbones. The resulting maps support interactive robotic perception and natural-language querying without additional training, enhancing potential for practical deployment in dynamic environments. Current limitations include dependence on captioning and detection backbone quality, occasional semantic drift in challenging scenes, and computational overhead from vision-language models and high-resolution mapping. Future work will focus on better semantics-geometry integration, lighter labeling models for on-device use, improved temporal reasoning for long-term mapping, and testing in outdoor and manipulation scenarios.

REFERENCES

- G. Narita, T. Seno, T. Ishikawa, and Y. Kaji, "Panopticfusion: Online volumetric semantic mapping at the level of stuff and things," in 2019 IEEE/RSJ International Conference on Intelligent Robots and Systems (IROS). IEEE, 2019, pp. 4205–4212.
- [2] J. McCormac, R. Clark, M. Bloesch, A. Davison, and S. Leutenegger, "Fusion++: Volumetric object-level slam," in 2018 international conference on 3D vision (3DV). IEEE, 2018, pp. 32–41.
- [3] R. F. Salas-Moreno, R. A. Newcombe, H. Strasdat, P. H. Kelly, and A. J. Davison, "Slam++: Simultaneous localisation and mapping at the level of objects," in Proceedings of the IEEE conference on computer vision and pattern recognition, 2013, pp. 1352–1359.
- [4] F. Li, H. Zhang, H. Xu, S. Liu, L. Zhang, L. M. Ni, and H.-Y. Shum, "Mask dino: Towards a unified transformer-based framework for object detection and segmentation," in Proceedings of the IEEE/CVF Conference on Computer Vision and Pattern Recognition, 2023, pp. 3041–3050.
- [5] Z. Zong, G. Song, and Y. Liu, "Detrs with collaborative hybrid assignments training," in <u>Proceedings of the IEEE/CVF International</u> Conference on Computer Vision, 2023, pp. 6748–6758.
- [6] K. Mazur, E. Sucar, and A. J. Davison, "Feature-realistic neural fusion for real-time, open set scene understanding," in 2023 IEEE International Conference on Robotics and Automation (ICRA). IEEE, 2023, pp. 8201–8207.
- [7] K. M. Jatavallabhula, A. Kuwajerwala, Q. Gu, M. Omama, T. Chen, A. Maalouf, S. Li, G. S. Iyer, N. V. Keetha, A. Tewari, J. B. Tenenbaum, C. M. de Melo, M. Krishna, L. Paull, F. Shkurti, and A. Torralba, "Conceptfusion: Open-set multimodal 3d mapping," in <u>ICRA2023 Workshop</u> on Pretraining for Robotics (PT4R), 2023.
- [8] L. Schmid, J. Delmerico, J. L. Schönberger, J. Nieto, M. Pollefeys, R. Siegwart, and C. Cadena, "Panoptic multi-tsdfs: a flexible representation for online multi-resolution volumetric mapping and longterm dynamic scene consistency," in <u>2022 International Conference on</u> Robotics and Automation (ICRA). IEEE, <u>2022</u>, pp. 8018–8024.
- [9] A. Rosinol, M. Abate, Y. Chang, and L. Carlone, "Kimera: an opensource library for real-time metric-semantic localization and mapping," in 2020 IEEE International Conference on Robotics and Automation (ICRA). IEEE, 2020, pp. 1689–1696.
- [10] T. Hu, J. Jiao, Y. Xu, H. Liu, S. Wang, and M. Liu, "Dhp-mapping: A dense panoptic mapping system with hierarchical world representation and label optimization techniques," in 2024 IEEE/RSJ International Conference on Intelligent Robots and Systems (IROS). IEEE, 2024, pp. 1101–1107.
- [11] J. McCormac, A. Handa, A. Davison, and S. Leutenegger, "Semanticfusion: Dense 3d semantic mapping with convolutional neural networks," in 2017 IEEE International Conference on Robotics and automation (ICRA). IEEE, 2017, pp. 4628–4635.
- [12] Y. Xiang and D. Fox, "Da-rnn: Semantic mapping with data associated recurrent neural networks," in <u>Robotics: Science and Systems (RSS)</u>, 2017

- [13] H. Zhang, F. Li, X. Zou, S. Liu, C. Li, J. Yang, and L. Zhang, "A simple framework for open-vocabulary segmentation and detection," in Proceedings of the IEEE/CVF International Conference on Computer Vision, 2023, pp. 1020–1031.
- [14] X. Li, H. Yuan, W. Li, H. Ding, S. Wu, W. Zhang, Y. Li, K. Chen, and C. C. Loy, "Omg-seg: Is one model good enough for all segmentation?" in Proceedings of the IEEE/CVF Conference on Computer Vision and Pattern Recognition, 2024, pp. 27948–27959.
- [15] X. Huang, Y. Zhang, J. Ma, W. Tian, R. Feng, Y. Zhang, Y. Li, Y. Guo, and L. Zhang, "Tag2text: Guiding vision-language model via image tagging," in <u>International Conference on Learning Representations</u> (ICLR), 2024.
- [16] S. Liu, Z. Zeng, T. Ren, F. Li, H. Zhang, J. Yang, Q. Jiang, C. Li, J. Yang, H. Su et al., "Grounding dino: Marrying dino with grounded pre-training for open-set object detection," in <u>European conference on</u> computer vision. Springer, 2024, pp. 38–55.
- [17] A. Kirillov, E. Mintun, N. Ravi, H. Mao, C. Rolland, L. Gustafson, T. Xiao, S. Whitehead, A. C. Berg, W.-Y. Lo et al., "Segment anything," in Proceedings of the IEEE/CVF international conference on computer vision, 2023, pp. 4015–4026.
- [18] Q. Gu, A. Kuwajerwala, S. Morin, K. M. Jatavallabhula, B. Sen, A. Agarwal, C. Rivera, W. Paul, K. Ellis, R. Chellappa et al., "Concept-graphs: Open-vocabulary 3d scene graphs for perception and planning," in 2024 IEEE International Conference on Robotics and Automation (ICRA). IEEE, 2024, pp. 5021–5028.
- [19] S. Lu, H. Chang, E. P. Jing, A. Boularias, and K. Bekris, "Ovir-3d: Open-vocabulary 3d instance retrieval without training on 3d data," in Conference on Robot Learning. PMLR, 2023, pp. 1610–1620.
- [20] A. Takmaz, E. Fedele, R. W. Sumner, M. Pollefeys, F. Tombari, and F. Engelmann, "OpenMask3D: Open-Vocabulary 3D Instance Segmentation," in <u>Advances in Neural Information Processing Systems (NeurIPS)</u>, 2023.
- [21] H. Caesar, J. Uijlings, and V. Ferrari, "Coco-stuff: Thing and stuff classes in context," in Proceedings of the IEEE conference on computer vision and pattern recognition, 2018, pp. 1209–1218.
- [22] M. Honnibal, "A good part-of-speech tagger in about 200 lines of python," https://explosion.ai/blog/part-of-speech-pos-tagger-in-python, 2013
- [23] C. Fellbaum, "Wordnet," in <u>Theory and applications of ontology:</u> computer applications. Springer, 2010, pp. 231–243.
- [24] K. Song, X. Tan, T. Qin, J. Lu, and T.-Y. Liu, "Mpnet: Masked and permuted pre-training for language understanding," Advances in Neural Information Processing Systems, vol. 33, pp. 16857–16867, 2020.
- [25] J. Johnson, M. Douze, and H. Jégou, "Billion-scale similarity search with gpus," <u>IEEE Transactions on Big Data</u>, vol. 7, no. 3, pp. 535–547, 2019
- [26] R. Girshick, J. Donahue, T. Darrell, and J. Malik, "Rich feature hierarchies for accurate object detection and semantic segmentation," in <u>Proceedings of the IEEE conference on computer vision and pattern</u> recognition, 2014, pp. 580–587.
- [27] A. Dai, A. X. Chang, M. Savva, M. Halber, T. Funkhouser, and M. Nießner, "Scannet: Richly-annotated 3d reconstructions of indoor scenes," in Proceedings of the IEEE conference on computer vision and pattern recognition, 2017, pp. 5828–5839.
- [28] J. Wald, A. Avetisyan, N. Navab, F. Tombari, and M. Nießner, "Rio: 3d object instance re-localization in changing indoor environments," in Proceedings of the IEEE/CVF International Conference on Computer Vision, 2019, pp. 7658–7667.
- [29] A. Gupta, P. Dollar, and R. Girshick, "Lvis: A dataset for large vocabulary instance segmentation," in <u>Proceedings of the IEEE/CVF</u> <u>conference on computer vision and pattern recognition</u>, 2019, pp. 5356– 5364
- [30] Y. Wu, A. Kirillov, F. Massa, W.-Y. Lo, and R. Girshick, "Detectron2," https://github.com/facebookresearch/detectron2, 2019.